CHAPTER 5

DESIGN ASPECTS AND STABILITY STUDY OF SECOND HARMONIC GYRO-TWT AMPLIFIER

5.1. Introduction

The gyro-TWT amplifier is an efficient coherent high-power microwave and millimeter-wave source with a wide variety of applications ranging from high-resolution radar to high-information density communications systems, while its performance is severely deteriorated by the stability (spurious oscillations) problems. The interaction circuit of gyro-TWT is intrinsically rugged due to its fast-wave interaction in unloaded waveguide. In a gyro-TWT amplifier, electrons gyrate along an axial magnetic field tuned so that they interact synchronously with and continuously amplify a copropagating electromagnetic wave.

Gyro-TWT amplifier is susceptible to spurious oscillations. The spurious oscillations in a gyro-TWT interaction region are divided into two groups, namely, external feedback induced oscillations (reflective oscillation) and internal feedback induced oscillations (absolute instability, gyrotron backward oscillation) [Lau *et al.* (1981), Barnett *et al.* 1989, Chu *et al.* 1998, Chu *et al.* 1999)]. The mismatches at the input port and output port of the circuit reflect the output power back into the interaction region. When the loop gain over more then sum of the dissipated power and end reflections, an external feedback induced oscillation will be built up. For supressing the external feedback induced oscillations well matched input-output couplers with the device [Chu (2004)]. The internal feedback induced oscillations (absolute instability, gyrotron backward oscillation) are inherent within the gyro-TWT, which are caused by the strong couplings between the cyclotron harmonics and synchronized guided modes.

The absolute instability occurs when the low frequency end of the unstable band in the forward-wave region merges with the normally evanescent backward wave region. The

lowest threshold current of the absolute instabilities is higher than the operating current, which brings the system high stability. Gyro-BWO occurs if the interaction of beam mode and waveguide mode when $k_z < 0$. To avoid gyro-BWO the interaction circuit must be kept shorter than the start-oscillation length to ensure amplification in the operating mode. For reducing the length, multi-stage system is preferred.

The operating frequency of gyro-TWT is directly proportional to the applied DC magnetic field. The availability of magnetic field places an upper limit on the frequency which can be amplified by a fundamental harmonic gyro-TWT. Because of its strong interaction, a fundamental harmonic gyro-TWT amplifier is also quite susceptible to spontaneous oscillations. Most of the gyro-TWTs developed in the past have operated at the fundamental cyclotron harmonic. For reducing the magnetic requirement and high power level gyro-TWT has operated at higher cyclotron harmonics. There are significant advantages to using higher harmonics [Wang *et al.* 2000]. The harmonic operation reduces the required magnetic field strength by a factor of the harmonic number s.

By using the harmonic resonance condition, the equations of motion, and the cutoff frequency relation, for operation close to cutoff, the value of $v_{mn} r_L / r_w$ is approximately equal to β_t, where β_t is normalized transverse velocity. For $\beta_t^2 \ll 1$, can be represented by the leading term of its series expansion, $J_s'^2(s\beta_t) = 0.25(s\beta_t/2)^{2(s-1)} / (s!)^2$. For small values of β_t, $J_s'^2(s\beta_t)$ becomes considerably weaker for higher harmonics. For harmonic gyro-TWT the threshold beam current is increases [Wang *et al.* (2000)]. In addition, gyro-TWT amplifiers can stably operate at higher beam current and, therefore, produce higher power at higher harmonics. This is because the weaker harmonic interactions yield a higher

threshold electron beam current for the absolute instability at the cutoff frequency of the operating mode.

In this chapter, proposing the use of wedge-shaped lossy ceramic rods symmetrically arranged on the inner wall of the cylindrical waveguide. Such an arrangement provides resistive loss to the azimuthally asymmetric modes while supporting azimuthally symmetric modes as long as the lossy ceramic rods remains thin. By optimising the lossy ceramic rods dimension, this type of structure ensures device stability by suppressing backward wave oscillations (BWO) in the gyro-TWT amplifiers. The rest of this article is organized as follows. In section 5.2, the design and stability of the harmonic gyro-TWT is discussed. In section 5.3, analysis of gyro-BWOs and RF interaction circuit design considerations have been discussed using distributed loss technique. Section 5.4 presents the beam-wave interaction behavior and parametric analysis of a harmonic gyro-TWT is discussed. The validation of nonlinear analysis through PIC simulation is discussed in section 5.5 and the results are explained in the succeeding section 5.6. Finally, the conclusion of the chapter is drawn in section 5.6.

5.2. Design and Stability Analysis of Second Harmonic Gyro-TWT Amplifier

The gyro-TWT is mainly consisting of MIG (magnetron injection gun), interaction structure and collector. Figure 5.1 illustrates cross-sectional view, efficiency and schematic of gyro-TWT amplifier uisng wedge shaped dielectric loaded RF interaction structure. For the stability, the interaction region of gyro-TWT amplifier is loaded with a ceramic material (BeO-SiC) has wedge shape. For sufficient attenuation of reducing the gyro-BWO, total number of six wedges is used with azimuthal symmetry is around 1.27mm width, 72mm long and the total interaction length is 100mm. A hollow beam of electrons comprised of

helical beamlets of small orbital radii compared to the transverse dimensions of the interaction structure of the device, is formed normally by an electron gun, called the magnetron injection gun (MIG) [Singh (2008)].

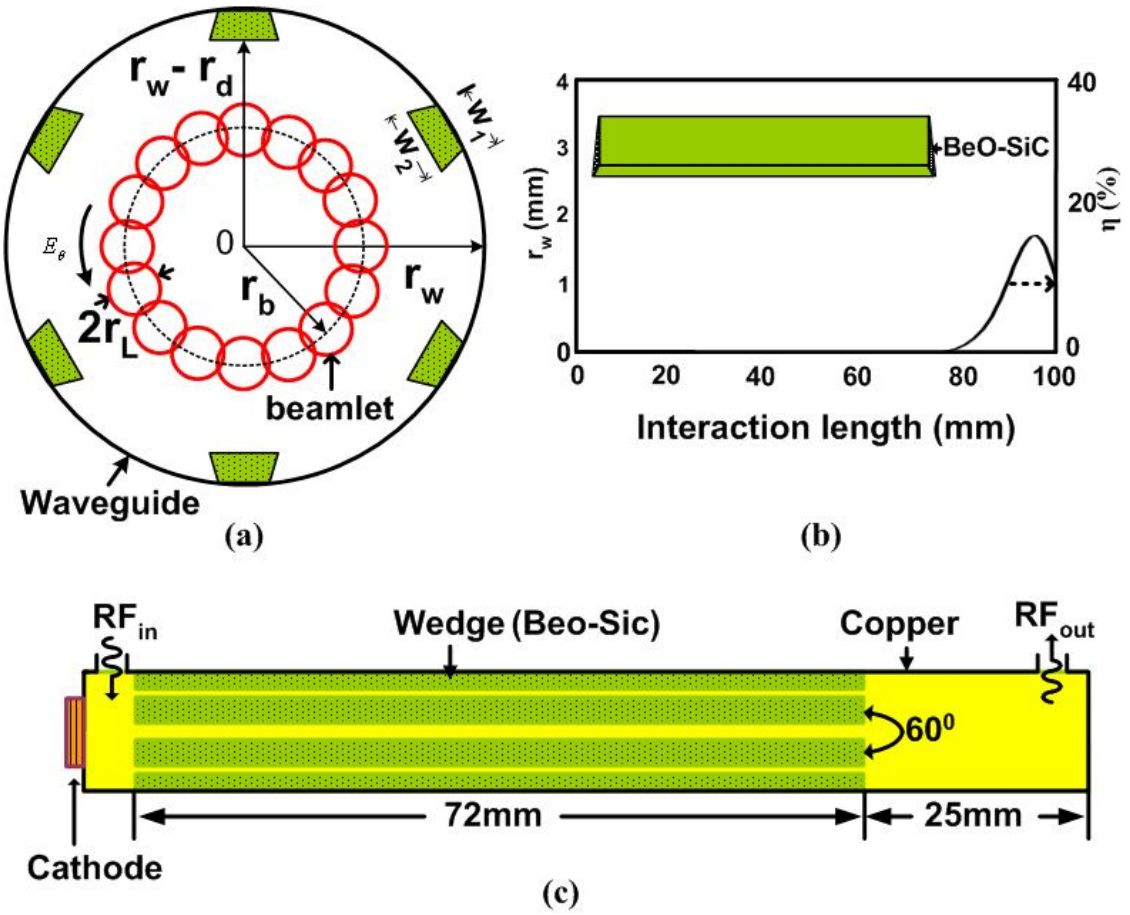

Figure 5.1. (a) Cross-sectional view, **(b)** Efficiency of W-band gyro-TWT amplifier, and **(c)** Schematic of the tube using wedge shaped dielectric loaded RF interaction structure.

The ECM instability in the gyro-TWT is characterized by a dispersion relation $D(\omega, k_z) = 0$, which determines how an initial disturbence will grow in linear stage. Instabilities are generally classified into two types: convective and absolute. Although the convective instability is desirable in a gyrotron amplifier system, diverse instabilities blossom under different operating conditions. The most hazardous effects are the absolute

instability near the cut-off frequency of the operating mode, the backward wave oscillations, and the reflective oscillations [Wang *et al.* (2011)]. The absolute and gyro-BWO instabilities phenomena are fundamentally understood with the help of cold (electron beam absent) or small signal dispersion relation, as shown in Fig. 5.2.

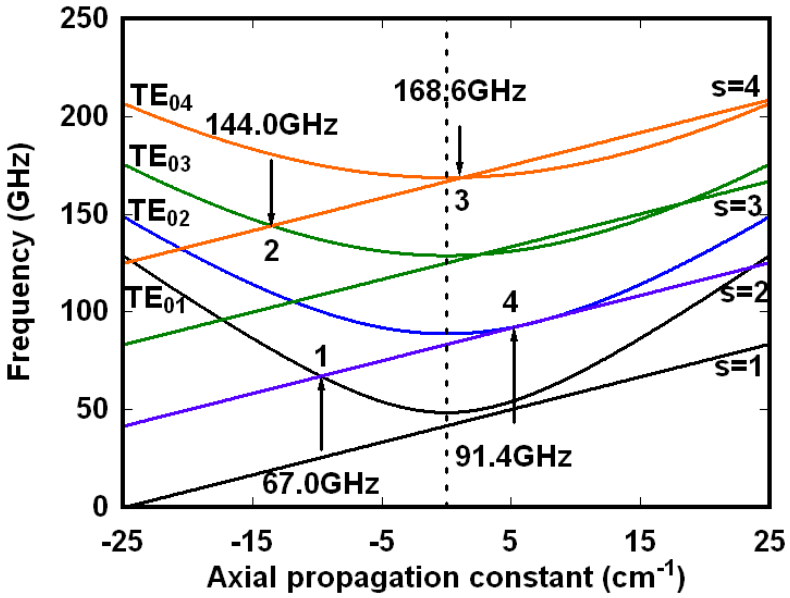

Figure 5.2. Dispersion diagrams of 91.4GHz gyro-TWT amplifier.

5.2.1. *Mode selection*

Gyro-TWTamplifier operation at the specific frequency, it is necessary that the device should work in that desired mode. The device operation in the parasitic modes results in a shift in its operating frequency and also a decrease in the efficiency. The choice of operating mode depends on the ohmic wall losses, mode competition, feasibility of the electron gun cathode design and coupling coefficient. For the operation in TE_{mn} mode [Liao (1985)], the waveguide wall radius r_w is related to λ by

$$r_w = \frac{v_{mn}\,\lambda}{2\pi} \tag{5.1}$$

where, v_{mn} is the n^{th} root of the first derivative of Bessel function $J'_m(x) = 0$.

5.2.2. *Magnetic field*

Applied external magnetic field employ as beam focussing and transport as well as provides necessary means for the beam-wave coupling occur. For maintain an efficient resonance between the beam and the wave magnetic field requires possessing good uniformity along the propagation direction. To avoid interaction of the gyro-TWT in backward region $(k_z < 0)$ device operate at grazing condition. The grazing condition is when the axial velocity of the beam is equal to the group velocity of the RF wave. With the help of fine tuning of magnetic field, achieve grazing interaction [Chu and Lin 1998]. The grazing magnetic field B_g is defined as,

$$B_g = \frac{\gamma_0 \omega_c m_0}{e \gamma_{z0} s} \tag{5.2}$$

and (ω_g, k_{zg}) is the point of grazing interaction where $\omega_g = \gamma_{z0}\omega_c$, $k_{zg} = \gamma_{z0}\beta_z \nu_{mn}$, $\omega_c = k_{mn}c.$

5.2.3. *Coupling Coefficient*

The coupling coefficient determines the strength of the electron beam coupling to the RF mode and depends on the electron beam guiding centre radius and the electric field distribution for a particular mode. The coupling co-efficient should be maximum for the desired mode, so that the desired mode can be excited during the device operation. Once the desired mode is excited properly by the helical moving electron beam, the other competing modes are suppressed, and power growth mechanism gets single mode stability [Sinitsyn *et al.* (2002)]. The coupling coefficient between the electron beam and RF wave in the cylindrical waveguide is defined as,

$$C_{mn} = \frac{J_{m\pm s}^2(k_t r_b)}{(\nu_{mn}^2 - m^2) J_m^2(\nu_{mn})} \tag{5.3}$$

where, $k_t = 2\pi/\lambda$, r_b is the beam radius, v_{mn} is the eigen value of the mn mode.The normalized coupling coefficient (C_{mn}) with respect to the normalized beam radius for the different modes is shown in Fig. 5.3, design parameter are given in Table 5.1.

It can be seen from the Fig. 5.3, that the normalized coupling coefficient G_{cpl} between the electron beam and RF field in the waveguide in case of TE_{02} second harmonic mode is much larger than that of all other modes. So, in order to have the maximum interaction between the electron beam and the electromagnetic field, the TE_{02} mode is chosen as the operating mode. The first radial maximum of TE_{01} mode, which is equal to normalized beam radius and found as 0.44, is the normalized beam position for maximum coupling. However, to reduce the interaction strength of the competing TE_{01}^{2}, TE_{02}^{3} *and* TE_{03}^{4} modes, a value for of 0.41 was chosen for the design. The coupling for the operating *TE* mode is still near its maximum.

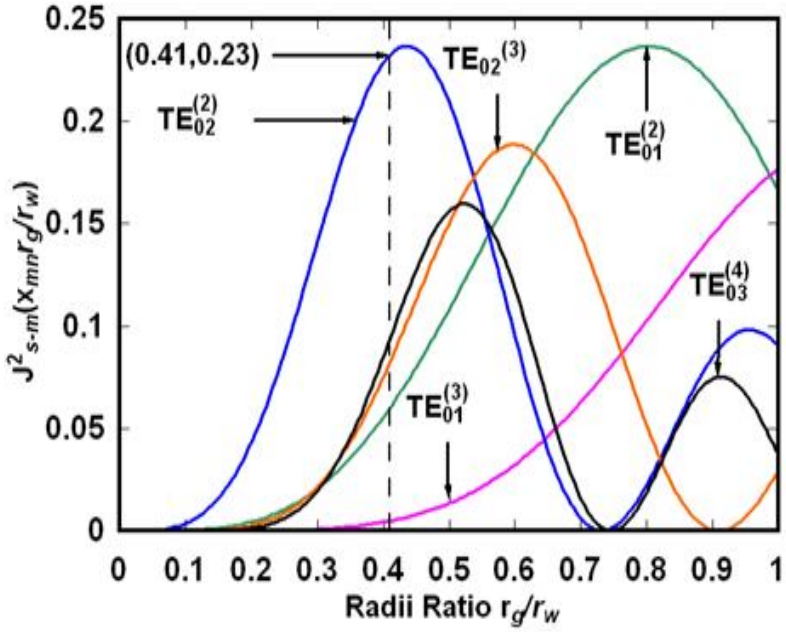

Figure 5.3. Dependence of the gyro-TWT amplifier coupling coefficient on guiding-center radius.

The cold dispersion relation [Sirigiri (1999)] basically refers the conditions at which the absolute instability is excited and also accounts the required loss for maintaining the stability of the device. The gyro-BWO results from the interaction between a helically moving gyrating electrons and the counter propagating RF wave. The cold dispersion relation is a complex solution of angular frequency (ω) for the real value of wave number (k), and vice-versa, as shown in Fig. 5.2.

It shows the intersection of the circular TE_{01} mode with the beam mode, s = 2 line (at 67.57 GHz) and TE_{03} with s = 4 line (at 144.34 GHz). These are referred as the backward wave oscillation modes excited due to the internal reflection mechanism and having negative wave number travelling in the backward direction. Further, the forward intersection (positive wave number) of the TE_{04} mode with s = 4 line denotes the transition of convective instability into an absolute instability at 168.6GHz. Figure 5.2 also shows the optimum operating point of the second harmonic TE_{02}-mode gyro-TWT at 91.4GHz with the beam parameters of 100kV, 25A, and the pitch factor of 1.2.

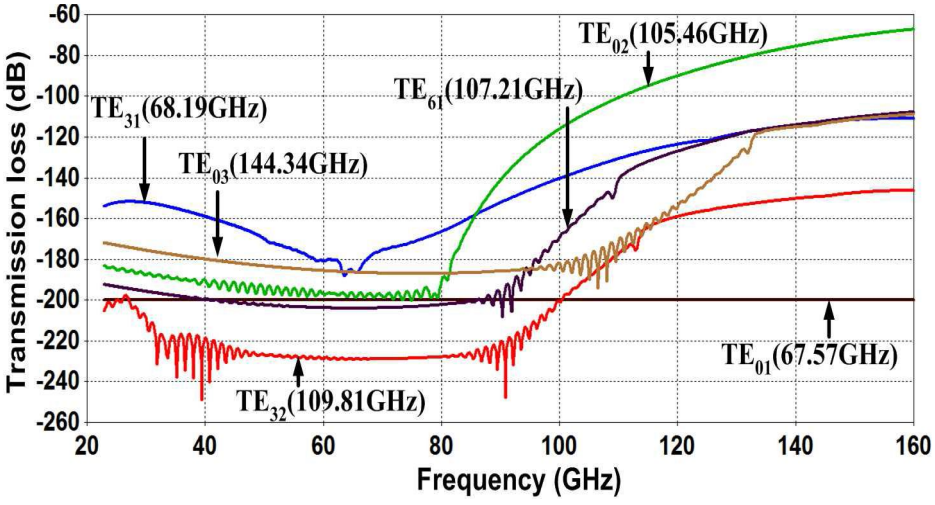

Figure 5.4. Transmission loss of the desired TE_{02} mode and its competing nearby modes.

In order to ensure stable gyro-TWT device operation, its RF interaction section is loaded with the wedge shaped lossy ceramic rods. To study the stability condition of such lossy structure, this circuit is modeled and cold tested for its propagation characteristics, as shown in Fig. 5.3 using "CST Microwave Studio" [CST user's manual (2014)]. The propagation loss of azimuthally asymmetric modes of interest including TE_{31}, TE_{61}, and TE_{32} are obtained as 21dB /cm, 27dB /cm, and 30dB /cm, respectively. Similarly, the loss for the azimuthally symmetric modes of interest including TE_{01}, and TE_{03} are obtained as 28dB /cm, and 25dB /cm, respectively. These are spuriously competing with the operational TE_{02} mode at 91.4 GHz. Further, the loss tangent of the lossy dielectric is varied to observe the variation of the transmission loss for the desired and nearby competing modes, as shown in fig. 5.4. The loss tangent is defined as,

$$\tan\delta = \frac{\varepsilon''}{\varepsilon'} = \frac{\sigma}{\omega\varepsilon_0\varepsilon'} \tag{5.4}$$

Where ε' and ε'' is the real and imaginary part of complex dielectric constant, ε_0 (dielectric constant of vacuum) is permittivity and σ is the conductivity of the material. The loss for the desired TE_{02}^2 operating mode is obtained as ~19dB /cm at 91.4 GHz for the loss tangent of 0.154 with the layer thickness of d =1.27 mm. The $\varepsilon''/\varepsilon'$ term describes how much energy supplied by an external electric field is dissipated as motion and heat.

Further, the loss tangent of the lossy dielectric is varied to observe the variation of the transmission loss for the desired and nearby competing modes, as shown in Fig. 5.5. The loss for the desired TE_{02}^2 operating mode is obtained as ~19dB /cm at 91.4GHz for the loss tangent of 0.154 with the layer radial thickness (r_d) of 1.27mm.

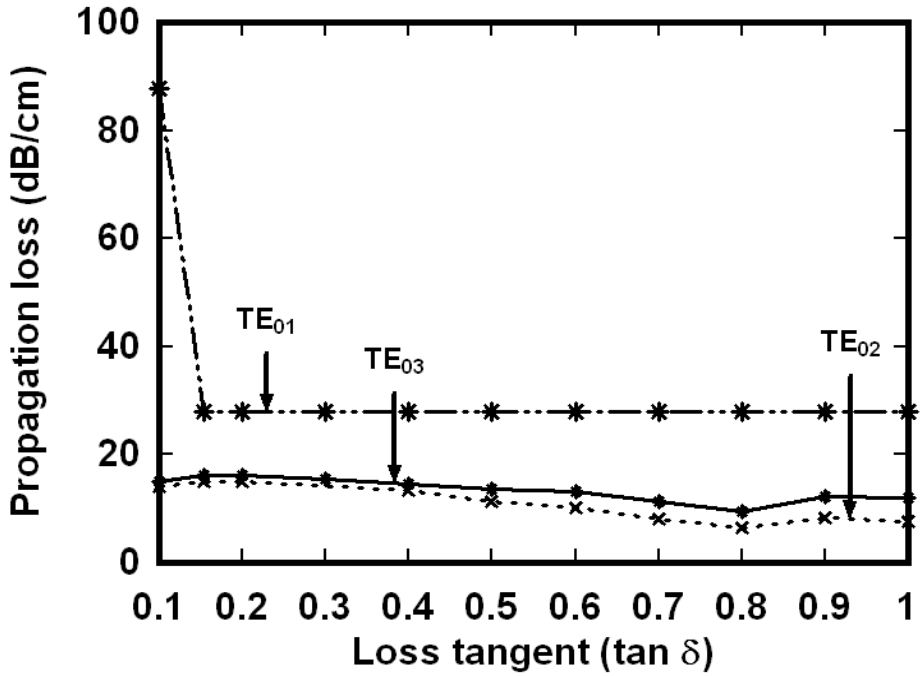

Figure 5.5. Variation of transmission loss versus loss tangent.

5.2.4. *Start Oscillation Current*

For device operation in the desired mode, the start up scenario is examined which should fulfil the conditions of self-excitation. This would lead to the nominal operating point in a way that ensures the desired mode excitation with maximum efficiency at the desired output power, while neighbouring modes are suppressed. Among all of the gyro-devices gyro-TWT has highly susceptible to self oscillations (absolute instability, gyro-BWO, and reflective oscillation). To avoid absolute oscillation drive current must be less then a critical current. This critical current is called start oscillation current which is a function of various operating parameters (such as the beam voltage, beam radius, beam velocity ratio, etc). The critical current can be calculated using a linearized single mode theory. Above critical current device produce self-oscillation. For proper stable amplification drive current must be less then critical current.

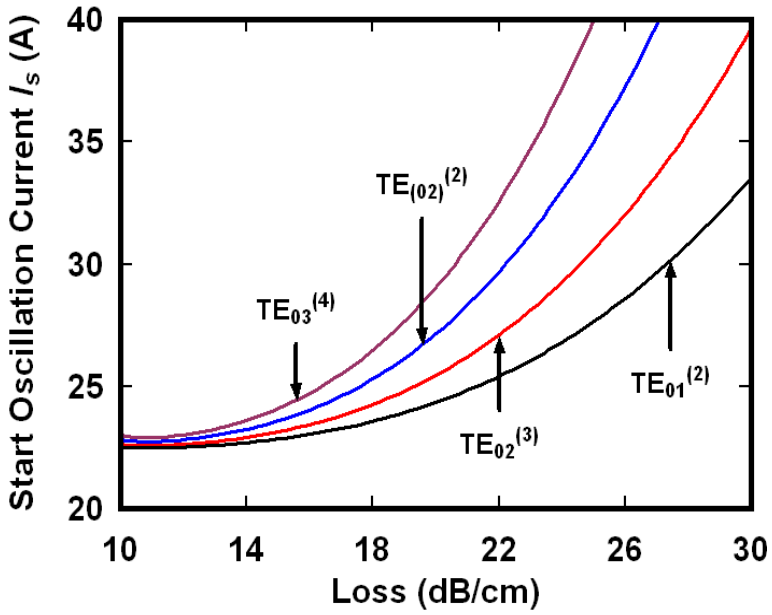

Figure 5.6. Start oscillation current vs transmission loss for the desired and spurious modes.

Figure 5.6 shows the variation of the start oscillation current with respect to the transmission loss for the desired TE_{02}^{2} , and its rivals TE_{01}^{2} , TE_{02}^{3} and TE_{03}^{4} modes. As the loss approaching ~ 18dB /cm, the start current exceeds 26A for the operating TE_{02}^{2} mode. The design constraint includes threshold of the electron beam current, above which absolute instability occurs and below which the convective amplification takes place. Therefore, to improve the stability and maximize the RF output power, the device must be operated below the threshold value.

5.2.5. *Harmonic Effect*

In addition to the instability and oscillations (absolute instability, gyro- BWO and reflective oscillation) problem the fundamental harmonic gyro-TWT required strong magnetic field at millimetre and sub-millimetre frequency, because the amplified frequency of RF wave is directly proportional to magnetic field through $\omega \simeq \Omega = 1.76 \times 10^{11} B_0(\mathrm{T}) / \gamma$. A very simple solution is to operate the gyro-TWT at the s^{th} harmonic of the cyclotron

frequency and thereby reduced the required magnetic field by a factor of *s* [Wang 1995]. For the resonant interaction of circular waveguide TE_{mn} mode with sinusoidal time dependence of the form

$$E \sim \cos(m\Phi - \omega t + k_z z + \Phi_o) \tag{5.5}$$

The phase of the field is defied as,

$$m\Phi - \omega t + k_z z + \Phi_o = \text{constant} \tag{5.6}$$

Taking the derivative with respect to time, and taking $d\Phi/dt$, we obtains

$$\omega = k_z v_z + m\Omega \quad . \tag{5.7}$$

Thus, if a harmonic gyro-TWT is designed such that the cyclotron harmonic number *s* equals the field azimuthal modes number the magnet is field required amplifying a given RF frequency is reduced by a factor of *s*. However, the harmonic interaction is weaker then the fundamental harmonic interaction for the same strength of the RF fields in the waveguide.

The high harmonic operation reduces the magnetic strength and possibly replaces the superconducting magnet by a normal compact coil magnet. A gyro-TWT based on normal coil definitely enhances the system reliability and shortens the start-up time of the radar system for military application. It is realized that since harmonic interactions are weaker in general than the fundamental interaction and that harmonic gyro-TWT are more stable to oscillation so that the oscillation threshold current level is much higher. This leads to the possibility for high beam current operation and significantly higher beam power available for amplification in a harmonic gyro-TWT than in a fundamental gyro-TWT, while amplifier stability is still maintained as long as the interaction length is also kept shorter than the critical length for gyro-BWO oscillation to start. In general, a harmonic gyro-TWT

has higher threshold current because of the weaker harmonic interaction. Therefore, the available excess energy of electrons boosts up the amplification in harmonics operation of the gyro-TWT rather than the fundamental operation. Analytical expression [Chu and Lin (1988)] for the saddle point at the onset of the absolute instability and critical beam current for absolute instability

$$I_c = 1.152\times 10^5 \frac{\gamma_0 \beta_{z0}^3 v_{mn}^2 K_{mn}}{\beta_{t0}^2 H_{sm}\left(k_t r_g, k_t r_L\right)}\left(\frac{k_{zs}}{k_t}\right)^4 \tag{5.8}$$

$$k_{zs} = k_t\left(\frac{\omega_s}{\omega_c} - \frac{B_0}{B_g}\right)\Big/ 4\beta_{z0} \tag{5.9}$$

$$\omega_s = \omega_c\left\{\frac{B_0}{B_g} + \left[8\beta_{z0}^2\left(1-\frac{B_0^2}{B_g^2}\right) + 64\beta_{z0}^4\right]^{1/2}\right\}\Big/\left(1+8\beta_{z0}^2\right) \tag{5.10}$$

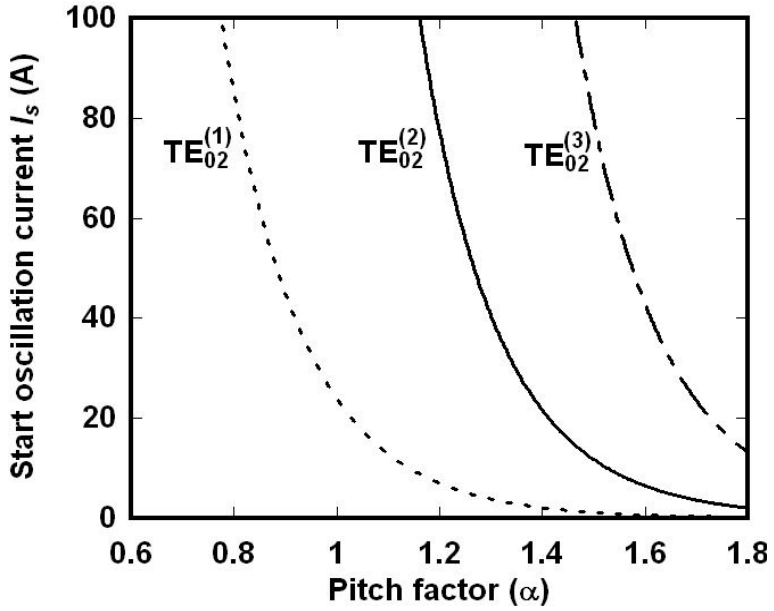

Figure 5.7. Variation of the start oscillation current with pitch factor with different harmonic.

Figure 5.7 shows the comparison of the start oscillation current in a third harmonic TE_{02}, second harmonic TE_{02} mode gyro-TWT and the fundamental TE_{02} mode of operation

for the absolute instability with the beam parameters of 100 kV, 25 A. This ensures that the second harmonic TE_{02} mode has higher value of start current than the fundamental operation for the velocity ratio (α) of 1.2. The RF output power and the efficiency increase as the pitch of the electron beam (α) increases due to the radiating energy is taken from the orbital motion of the electrons. However, the higher value of the pitch turns down the start oscillation current of the desired operating mode. Therefore, to achieve the stability and the saturation in high power devices, the reasonable value velocity ratio (α) should be around 1.

5.2.6. *Attenuation Constant*

The propagation constant γ is a complex quantity and is expressed as,

$$\gamma_a = k_A + jk_B \tag{5.11}$$

where k_A and k_B are the real and imaginary parts of γ_a and k_A is known as attenuation constant and is associated with the power losses in the structure. These losses may be due to dielectric and/or finite conductivity of structure walls. If the operating frequency is way below the cut-off frequency, the attenuation constant becomes very large and non-propagation occurs. For the frequencies greater than the cut-off frequency of the structure, the propagation constant γ_a is pure imaginary and is equal to jk_B if the medium is lossless inside the structure. But for our actual structure waveguide walls have some finite conductivity which results in finite wall power losses. Following the principle of conservation of energy, the attenuation constant accounting for the power loss along the structure can be expressed as,

$$k_A = \frac{\text{Time averaged power lost per unit length}}{2 \times \text{Time averaged power transmitted}} \tag{5.12}$$

The attenuation constant evaluated from dispersion equation by neglecting the beam term,

$$k_A = \frac{k_{mn}^2}{2k_{zr}} \frac{\delta}{r_w} \left(1 + \frac{m^2}{x_{mn}^2 - m^2} \left(\frac{\omega}{\omega_c} \right)^2 \right) \tag{5.13}$$

Hence in a unit distance along the waveguide, the amount of energy dissipated on the wall is $2k_A P_w$ and the energy input into the wave by the beam over the same distance is $2|k_{zi}| P_w$ and the quantities, η total power extracted from the beam divided by the beam power, η_w output wave power divided by the beam power, η_A total wall dissipated power divided by the beam power, we get

$$\eta_w = \frac{|k_{zi}|}{|k_{zi}| + |k_A|} \eta \qquad \text{and} \qquad \eta_A = \frac{|k_\Omega|}{|k_{zi}| + |k_A|} \eta \tag{5.14}$$

5.2.7. *Launching Loss*

In gyro-TWT, the interaction starts from input end and the wave spatially develops upto it reaches the output end. The input signal actually decompose into four waves (forward growing wave, forward decaying wave, forward constant wave, backward constant wave). Normally, the growing forward wave will become dominant after popagating several wavelengths. The ratio of the growing forward wave to the input signal is usually defined as the launching loss [Kou (1991)]. The launching loss is also defined as the difference between the total gain over the entire interaction length evaluated by using the four wave solution and by only using the growth rate of the forward growing wave. The launching loss significantly varies over the entire operating bandwidth and its a function of frequency for different values of magnetic field. Velocity spread can reduce the launching loss.

5.2.8. *Frequency width and growth rate*

The temporal growth rates for the instability at resonance are obtained by substituting $\omega = \omega_0 + \Delta\omega$ and $k_z = k_{z0}$ into dispersion equation, where (ω_0, k_0) is the point at which the waveguide characteristic curve

$$\omega^2 - k_t^2 c^2 - k_z^2 c^2 = 0 \tag{5.15}$$

and beam characteristic curve intersects,

$$\omega - k_z v_z - s\Omega / \gamma = 0 \tag{5.16}$$

evaluate $\Delta\omega = \Delta\omega_r + i\Delta\omega_i$ as follows

$$\Delta\omega_r = \left[\frac{v\, v_{mn}^2\, H_{sm}\, \beta_{t0}^2\, c^4}{4\, \gamma_0\, K_{mn}\, \omega_0\, r_w^4} \right]^{1/3} \tag{5.17}$$

where ω_r is the width of beam-wave interaction [Chu *et al.* (1980)]. The temporal growth rate is defined as,

$$\Delta\omega_i = \sqrt{3}\, \Delta\omega_r \tag{5.18}$$

where, $v = Nr_e = I_b(\mathrm{A}) / \left(1.707 \times 10^4 \beta_{z0}\right)$, N is the number of electrons per unit axial length and $\mathrm{r_e} = \mu_0 \mathrm{e}^2 / 4\pi m$, $\Delta\omega_r$ is the frequency width and $\Delta\omega_i$ is the temporal growth rate. From equation (5.18-5.19) shows that for a given electron beam and waveguide, the growth rate is highest for a wave near cut-off and approaches zero as the phase velocity approaches the free space value. In addition, the growth rate vanishes at grazing for TM modes ($v_z = v_g$). The spatial growth rate can be calculate by putting $\omega = \omega_0$ and $k = k_0 + \Delta k$ in dispersion relation, is defined as,

$$\Delta k_i = \left[\frac{1}{\beta_g \beta_{z0}^2}\right]^{1/3} \frac{\Delta\omega_i}{c} \tag{5.19}$$

where, Δk_i is the temporal growth rate [Wang (1995)].

5.2.9. *Wall Loading*

The RF power loss occurs due to finite conductivity of the materials used in the structure. For practical metallic structures, the metals like, copper, nickel, silver, etc. which are having very high conductivity are usually used. Ohmic loss is one of the major constraints in the operation of high power gyro-TWT [Chu *et al.* (1999)]. This RF power loss occurs in the waveguide as the ohmic heating due to the finite conductivity of the waveguide material and inserted lossy material. The RF power loss occurs due to finite conductivity of the materials used in the structure. For practical metallic structures, the metals like, copper, nickel, silver, etc. which are having very high conductivity are usually used.

$$P_{in} = -\int_0^{r_w} r dr \int_0^{2\pi} \left\langle \vec{J}.\mathrm{Re}\left(E\right)\right\rangle_t d\theta \quad \text{and} \quad P_{ohm} = \frac{1}{8}\omega\, x_{mn}^2\, K_{mn}\, \frac{\omega_c^2}{c^2}\frac{\delta}{r_w}\left(1+\frac{m^2}{x_{mn}^2-m^2}\right)\left|f\right|^2 \tag{5.20}$$

$$W_L(W/cm^2) = \frac{2.33\times10^{-3}\,P(\mathrm{W})}{v_{mn}^2\sqrt{\sigma}}\,\frac{f(\mathrm{GHz})^{5/2}}{\omega/\omega_c\sqrt{\omega^2/\omega_c^2-1}}\left[\frac{1}{\left(\omega/\omega_c\right)^2}+\frac{m^2}{v_{mn}^2-m^2}\right] \tag{5.21}$$

where P_{in} is the power per unit length deposited into the RF field by the electron beam, P_{ohm} is the Ohmic power per unit length dissipated on the wall, and $P(W)$ is the total power in watts, and σ is the conductivity in the interaction region of the device, the wall loading is a

function of the operating frequency to the cut-off frequency ratio [Wang (1995)]. Commonly accepted critical limit of wall loading is $2\,kW/cm^2$.

5.2.10. *Effect of Velocity Spread*

The electron beam velocity spread is an important aspect which should be incorporated to investigate the RF behavior of the device to have a more practical aspect. This is because during the experiments, 2% to 4% velocity spreads are always present due to which the electron beam quality degrades and as a result of this, both output power and efficiency of the device decreases. In order to take into account the velocity spread, its expedient to normalize all dimension parameters to the mean values of velocity components $\overline{\beta}_z$ and $\overline{\beta}_t$ and introduce coefficient k_F, k_μ, k_b and k_Δ describing the effect of the spread on these parameter [Sinitsyn *et al.* (2002), Tang *et al.* (2014)].

$$F = F_0 k_F, \qquad \overline{\mu} = \mu_0 k_\mu, \qquad b = b_0 k_b \tag{5.22}$$

$$\overline{\Delta} = k_0 \Delta_0 + k_0 h(\overline{\beta}_z - \beta_{z0}) \frac{1}{\beta_{z0}} \tag{5.23}$$

$$k_b = k_\mu = \frac{\overline{\beta}_z}{\beta_{z0}} \frac{1 - h\overline{\beta}_z}{1 - h\beta_{z0}} \left(\frac{\beta_{t0}}{\beta_t} \right)^2 \tag{5.24}$$

$$k_F = \frac{\overline{\beta}_z}{\beta_{z0}} \left(\frac{\beta_{t0}}{\beta_t} \right)^{s-2} \left(\frac{1 - h\overline{\beta}_z}{1 - h\beta_{z0}} \right)^{s-2} \tag{5.25}$$

$$k_\Delta = \frac{\overline{\beta}_z}{\beta_{z0}} \tag{5.26}$$

In the absence of the velocity spread, $k_b = k_F = \mathrm{k}_\Delta = 1$.

5.3. Analysis of Gyro-BWOs and RF Interaction Circuit Design Considerations

The operating TE_{02}^{2} mode is also prone to self-start oscillations caused due to the interaction of electron beam with the backward propagating modes including TE_{02}^{3}, TE_{01}^{2}, and TE_{03}^{4}, as shown in Fig. 5.2. If the RF circuit length exceeds the critical length, the backward wave oscillation (BWO) is self-excited. The stability against these backward wave oscillations is achieved by selecting the length of the RF circuit shorter than the critical length to get BWO to start.

Suppose physical circuit under consideration is a beam of relativistic electrons propagating along a circular waveguide under the influence of externally applied uniform magnetic field and interacting with a co-propagating circularly polarized TE_{mn} mode [Wang *et al.* (1992)]. The electron beam is tenuous whose distribution function in real and momentum space is expressed as

$$f\left(\mathrm{r},\mathrm{p},t\right)=f_0\left(\mathrm{r},\mathrm{p}\right)+f_1\left(\mathrm{r},\mathrm{p},t\right) \tag{5.27}$$

where

$$\left|f_1\left(\mathrm{r},\mathrm{p},t\right)\right|\ll\left|f_0\left(\mathrm{r},\mathrm{p}\right)\right| \tag{5.28}$$

Few assumptions have been taken in linear theory are in order:

1. *Space-Charge Effect Negligible*: For sufficient tenuous electron beam, the self field of the beam is much weaker than the RF fields available in the interaction region.
2. *Unaltered Transverse Field Pattern*: Due to sufficient tenuous electron beam, assume unaltered transverse field pattern.
3. *Single mode operation*: For exact synchronism electron beam interact with only one waveguide mode.

4. *Lossless Interaction Circuit*: For stability concerned, assume interaction circuit made up of a perfect conductor, all losses can be neglected.

The Maxwell-Vlasov equations are linearized to derive amplitude equations for the coupled waveguide modes in the small-signal regime. The amplitude equations are solved with the Laplace transform techniques, resulting in a dispersion relation with cyclotron harmonics. From Maxwell's wave equation,

$$\left(\frac{\partial^2}{\partial z^2}+k_z^2\right)A(\mathrm{z})=\Psi(\mathrm{z}) \tag{5.29}$$

Where $\Psi(\mathrm{z})$ the source term is defined as,

$$\Psi(z)=j\frac{4\pi\,k_t^2\omega C_{mn}}{c^2}\sum_{s=-\infty}^{\infty}\int_0^{2\pi}d\theta\int_0^{r_w}\left(r\,dr\,J_t(r,t)J_{m-s}(k_t r_b)J_s'\left(k_t r_L\right)e^{-j\varphi}\right) \tag{5.30}$$

The amplitude variable in wave equation is defined by the induced beam current. The induced beam current is produced by the RF field is described by perturbed distribution function $f_1(r,p,t)$ is defined as,

$$f_1(\mathrm{r},\mathrm{p},\mathrm{t})=\frac{eC_{mn}}{\omega}\sum_{s=-\infty}^{s=\infty}e^{j\varphi(\mathrm{t})}\int_0^z T_s(z-z')A_s(\mathrm{z}')dz' \tag{5.31}$$

Equation (5.35) is solved by the method of characteristics. The electron phase modulation represents an induced bean current, $J_t(\mathrm{r},\mathrm{t})$ is determined by electron distribution function. By putting the current value in wave equation, the amplitude $A(\mathrm{z})$ can be determined self-consistently by solving the resulting one-dimensional integro-differential equation. Appling the Laplace transformation and convolution theorem, wave equation reduced as,

$$\left(\frac{\omega}{c^2}^2-k_z^2-k_t^2\right)\widetilde{A}(\mathrm{k}_z)=\widetilde{\Psi}(\mathrm{k}_z)-\mathrm{j}\mathrm{k}_z\,A(0)+A'(0) \tag{5.32}$$

where,

$$A(0) = A(z)\big|_{z=0} \quad \text{and} \quad A'(0) = \frac{dA(z)}{dz}\bigg|_{z=0} \text{ are the initial conditions} \tag{5.33}$$

The source term $\widetilde{\Psi}(z)$ is defined as

$$\widetilde{\Psi}(k_z) = \Psi_1(k_z)\widetilde{A}(k_z) + \Psi_0(k_z)A(0) \tag{5.34}$$

Where,

$$\Psi_1(k_z) = \frac{16\pi^3\, e^2 k\, k_t\, C_{mn}^2}{m_0 c^2} \sum_{s=-\infty}^{\infty} \int_0^{r_b^{\max}} r_g\, dr_g \int_0^{\infty} p_t\, dp_t \int_{-\infty}^{\infty} dp_z \frac{f_0}{\gamma} \left[\frac{-\beta_{to}^2(\omega^2 - k_z^2 c^2)\, H_{sm}(k_t r_g, k_t r_L)}{\left(\omega - k_z v_{z0} - s\,\Omega_c/\gamma_o\right)^2} \right.$$

$$\left. + \frac{(\omega - k_z v_z)\, T_{sm}(k_t r_g, k_{mn} r_L) - k_{mn}\, v_t\, U_{sm}(k_t r_g, k_{mn} r_L)}{\omega - k_z v_{z0} - s\Omega_c/\gamma_o} \right] \tag{5.35}$$

$$\Psi_0(k_z) = \mathrm{j}\frac{16\pi^3 e^2\, k\, k_t C_{mn}^2}{m_0 c^2} \sum_{s=-\infty}^{\infty} \int_0^{r_b^{\max}} r_g\, dr_g \int_0^{\infty} p_t\, dp_t \int_{-\infty}^{\infty} dp_z\, \frac{f_0}{\gamma}$$

$$\left[\frac{-\beta_t^2\, \beta_{ph}^{-1}\, \omega\, H_{sm}(k_t r_g, k_t r_L)}{\left(\omega - k_z v_{z0} - s\,\Omega_c/\gamma_o\right)^2} + \frac{\beta_z T_{sm}(k_t r_b, k_t r_L)}{\omega - k_z v_{z0} - s\,\Omega_c/\gamma_0} \right] \tag{5.36}$$

and $$H_{sm}(x,y) = \mathrm{J}_{s-m}^2(x)\,\mathrm{J}_s'^2(y) \tag{5.37}$$

For a monoenergetic cold beam, the initial distribution function is defined as,

$$\mathrm{a}_0 = N_b \delta(\gamma - \gamma_0) \frac{1}{2\pi p_{to}} \delta(p_t - p_{t0}) \frac{1}{2\pi r_{bo}} \delta(r_t - r_b) \tag{5.38}$$

And by residue theorem, the field amplitude in real space can be expressed in initial value terms,

$$A(z) = A(0) \sum_i e^{-jk_{zi}z} \frac{N(k_{zi})}{j\,\mathrm{D}'(k_{zi})} + A'(0) \sum_i e^{-jk_{zi}z} \frac{1}{jD'(k_{zi})} \tag{5.39}$$

where

$$D(k_z) = \frac{\omega^2}{c^2} - k_z^2 - k_c^2 - \Psi_1(k_z) \quad \text{and} \quad D'(k_z) = \frac{dD}{dk_z} \tag{5.40}$$

$$N(k_z) = \Psi_0(k_z) - jk_z \tag{5.41}$$

The linear gain for forward wave $(k_z > 0)$ is defined as,

$$G(z) = \frac{P_w(z)}{P_w(0)} = \frac{\mathrm{Im}\{A(z)A'(z)^*\}}{\mathrm{Im}\{A(0)A'(0)^*\}} \tag{5.42}$$

And for backward wave $(k_z < 0)$ is given by

$$G(z) = \frac{P_w(0)}{P_w(z)} = \frac{\mathrm{Im}\{A(0)A'(0)^*\}}{\mathrm{Im}\{A(z)A'(z)^*\}} \tag{5.43}$$

By putting the boundary conditions in equation (5.47), (5.52) and (5.53) for forward travelling wave,

$$|A(0)| = \sqrt{\left(8\pi\omega\, k_t^2 \,/\, c^2 k_z\right) P_\omega(0)} \tag{5.44}$$

and $$A'(0)_{z=0} = -jk_z A(0) \tag{5.45}$$

and for backward wave

$$A'(0)\big|_{z=0} = jk_z A(0) \tag{5.46}$$

and $$Re\{A(z)\} + \mathrm{j}\, Im\{A(z)\} = 0\big|_{z=L}. \tag{5.47}$$

Linear forward gain can be defined by putting the value of amplitude of RF wave. By simultaneously solving backward wave equation wedged start oscillation length as well as oscillation frequency. When the real and imaginary part of backward wave are satisfied, the linear gain of backward wave is infinite, such that now amplifier work as a oscillator and defined the output at input end.

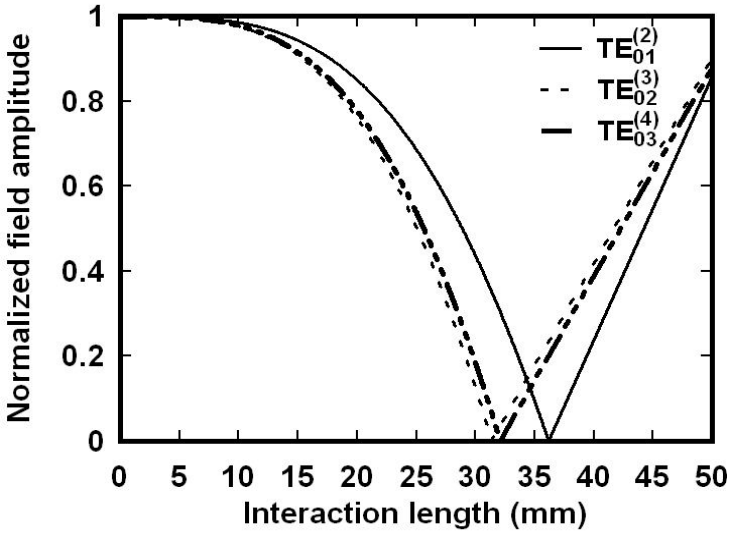

Figure 5.8. Origin of gyro-BWOs and their field variation along the RF interaction circuit.

By solving the equation (5.47), the frequency and critical length of the backward wave are calculated, as shown in Fig.5.8. The frequency of oscillations near the cyclotron resonance points (intersection of waveguide mode and beam mode lines, as shown in Fig. 5.2) are calculated for TE_{02}^{3}, TE_{03}^{4}, and TE_{01}^{2} as ~105GHz, ~144GHz, and ~67GHz, respectively. Figure 5.8 shows the amplitude of spurious BWO modes decreases and approaches zero at a distinctive point along the RF circuit length. The measure of the length at this point is called as the critical length to start the backward wave oscillation. The gain (equation (5.43)) of the amplifier at this point becomes infinite, if the field amplitude $A(z)$ in equation (5.47) satisfies the boundary conditions (5.45) and (5.46).

5.3.1. *Design Analysis and Performance Limiting Factor*

A major problem is gyro-BWO in gyro-TWT, it occurs when the beam-wave coupling is sufficient strong interaction at condition interaction at $k_z < 0$. In this condition RF wave can grow locally from noise without propagating axially out of the system. This oscillation therefore does not require external feedback. In order to avoid the instability, it's

necessary to restrict beam parameters such as the current and velocity ratio, which ultimately limits the overall efficiency. To avoid this problem recently developed marginal stability design criterion is applied to designing the interaction structure [Lin *et al.* (1992)]. According to this criterion interaction length must be less then critical length.This limits due to absolute instabilities can be obtained from the CRM linear dispersion expressed as,

$$D\left(\hat{\mathrm{k}},\hat{\omega}\right)=\left\{\hat{\omega}^2-\hat{k}^2-\left[1-(1+i)\left(1+\frac{m^2}{v_{mn}^2-m^2}\,\hat{\omega}^2\right)\frac{\delta}{r_w}\right]\right\}\left(\hat{\omega}-\hat{k}\,\beta_z-n b_c\right)^2+\varepsilon_c=0 \quad (5.48)$$

where $\hat{\omega}=\omega/\omega_c$, $\hat{k}=\hat{k}/k_t$ and $\omega_c=ck_t$. The quantity δ is the skin depth of waveguide wall. The quantity $b_c=\Omega_c/\omega_c$, where ω_c is the electron cyclotron frequency. For a beam with all electrons guiding centres located at guiding radius r_b. The ε_c is coupling constant as follow,

$$\varepsilon_c=\frac{4\beta_t^2}{\gamma_0\beta_z}\frac{\left[J_{m\pm n}\left(k_t r_g\right)\ \mathrm{J}_n'\left(k_t r_L\right)\right]^2}{\left(v_{mn}^2-m^2\right)J_m^2\left(v_{mn}\right)}\frac{I}{I_A} \quad (5.49)$$

where, I is the beam current, and $I_A=17.045kA$. For a given mode equation (5.49) indicates as $\beta_z\varepsilon_c$ should be as large as possible for increasing the allowable transverse beam energy, which scales as $\beta_t^2 I$.

Backward wave interaction is another critical oscillation in the analysis of the gyro-TWT amplifier's stability. BWO occurs when the beam-wave interaction at a negative k_z. The Backward mode will interrupt the amplifier if the starting threshold is exceeded [Hu (1997)]. Assume no energy or pitch angle spreads in the beam and match to appropriate boundary conditions at each end of the circuit give starting length $\hat{L}$ as,

$$\hat{L}^3 = \frac{2.06\beta_z^2\beta_{1/h}\chi(\mathrm{R})}{\varepsilon_c\left\{(1/h)^2-1\right\}^2} \tag{5.50}$$

where $\hat{L} = \omega L/c$, L is the interaction length. Equation indicates that the BWO is highly sensitivity to L. The parameter χ depends on R=R_1R_2, where R_1 and R_2 are the reflections at the ends of interaction region. The critical length for the three gyro-BWOs such as TE_{02}^3, TE_{03}^4, and TE_{01}^2 are calculated as ~31 mm, ~32 mm, and ~36 mm, respectively.

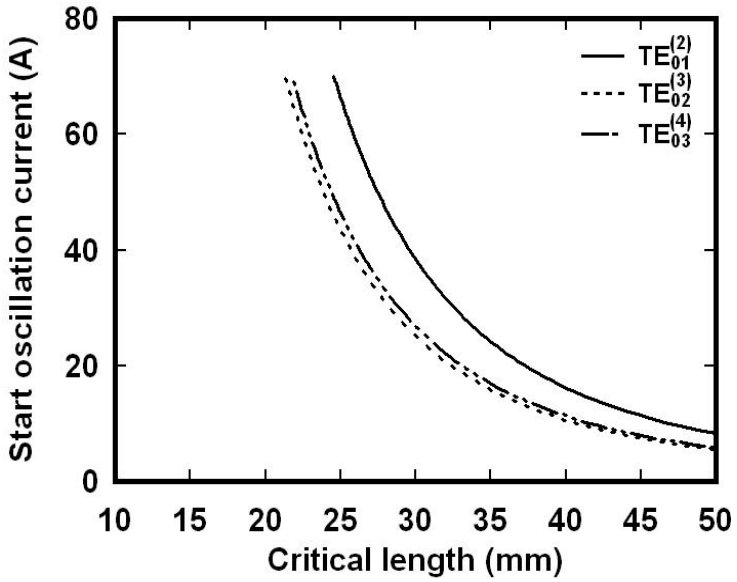

Figure 5.9. Dependence of start oscillation current on critical length.

The most vulnerable mode is the TE_{02}^3, that first limits the RF circuit length, as shown in Fig. 5.9. For properly working of gyro-TWT the interaction with competing mode must be suppressed. The beam current level where the unwanted oscillation takes place is called the "start-oscillation current", so that it is critical to operate the amplifier below I_s to ensure stability of the device. One way to increase I_s is to apply loss to the gyro-TWT circuit. The start oscillation current of lossy gyro-TWT amplifier can be expressed,

$$I_s = \frac{2k_b^4}{F_{mn}\,\varepsilon_v\,k_c^4}\left(0.0112\,\frac{\mathrm{L}_{dB}}{\mathrm{N}}\right)^3\left(1+\frac{1013}{L_{\mathrm{dB}}^2}\right)^3 \tag{5.51}$$

$$F_{mn} = \frac{J_{s-m}^2(k_{mn}r_b / r_w)}{k_{mn}^2 J_m^2(k_{mn})(1-m^2/\mathrm{k}_{mn}^2)} \tag{5.52}$$

$$\varepsilon_v = \frac{2.348\times10^{-4}}{\gamma\beta_z}\left(\frac{\beta_t}{\beta_z}\right)^2 J_1'\left(\frac{\beta_t\omega_c}{\Omega_r}\right)^2 \tag{5.53}$$

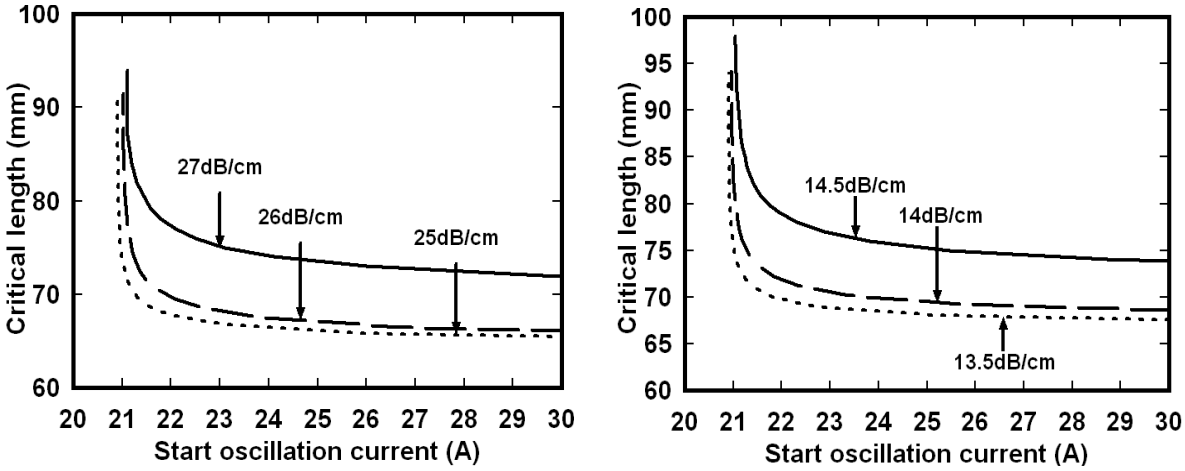

(a)

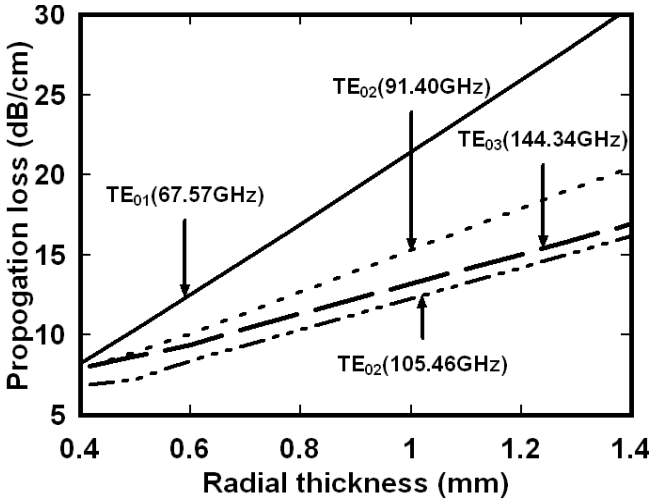

(b)

Figure 5.10. (a) Variation of the critical length with the start current for TE_{01}^2 and TE_{02}^3, and **(b)** propagation loss of operating and competing modes with respect to the thickness of wedge.

Table 5.1 Optimized design parameters of W-band second harmonic gyro-TWT amplifier

Parameters	Spectfication
Voltage	100kV
Current	25A
Operating mode	TE_{02}
Lossy layer thickness (r_d)	1.27mm
Cyclotron Harmonic	2
Velocity pitch factor ($\alpha=v_t/v_{z)}$	1.2
Velocity spread ($\Delta v_z/v_{z)}$	5%
Magnetic field, B_0	17.8kG
B_0/B_g	0.995
Circuit radius, r_w	0.377cm
Guiding center radius, r_g	$0.41*r_w$
circuit length	10cm

For the desired beam current of 25 A, the TE_{02}^3 mode has minimum critical length than other two modes that reduces the gain of the device. Therefore, the length of the nloaded (lossless) section is limited to ~ 25 mm in the present design and the lossy dielectric loading is used to maximize the gain of the gyro-TWT. Figure 5.10 (a) shows the variation of critical length of parasitic modes TE_{01}^2 at 67.57GHz and TE_{02}^3 at 105.46GHz for the different transmission losses, respectively. The critical lengths of TE_{01}^2 and TE_{02}^3 modes at 25A of current are calculated as 73.5 mm (27 dB/cm of loss) and 75 mm (14.5 dB/cm of loss) respectively.

Hence, the dielectric scheme of 72 mm to suppress the oscillations in the present design. Figure 5.10 (b) shows the variation of transmission loss of the operation mode and

other competing modes for the range of dielectric layer thickness. For the optimum thickness of 1.27 mm, the propagation loss is calculated for the desired TE_{02}^{2} mode as ~19 dB /cm. Other spurious modes including TE_{02}^{3}, TE_{01}^{2} and TE_{03}^{4} get attenuated at the rate of 15 dB/cm, 27.8 dB/cm and 15.8 dB/cm, respectively.

5.4. Analytical Results and Discussion

The small signal linear theory is used to analyse parasitic oscillations as described in section 5.2 that helps in selecting the circuit parameters. Further, the electrical parameters are chosen with respect to the design specifications of gyro-TWT amplifier. The analysis flow is shown in Fig. 5.11.

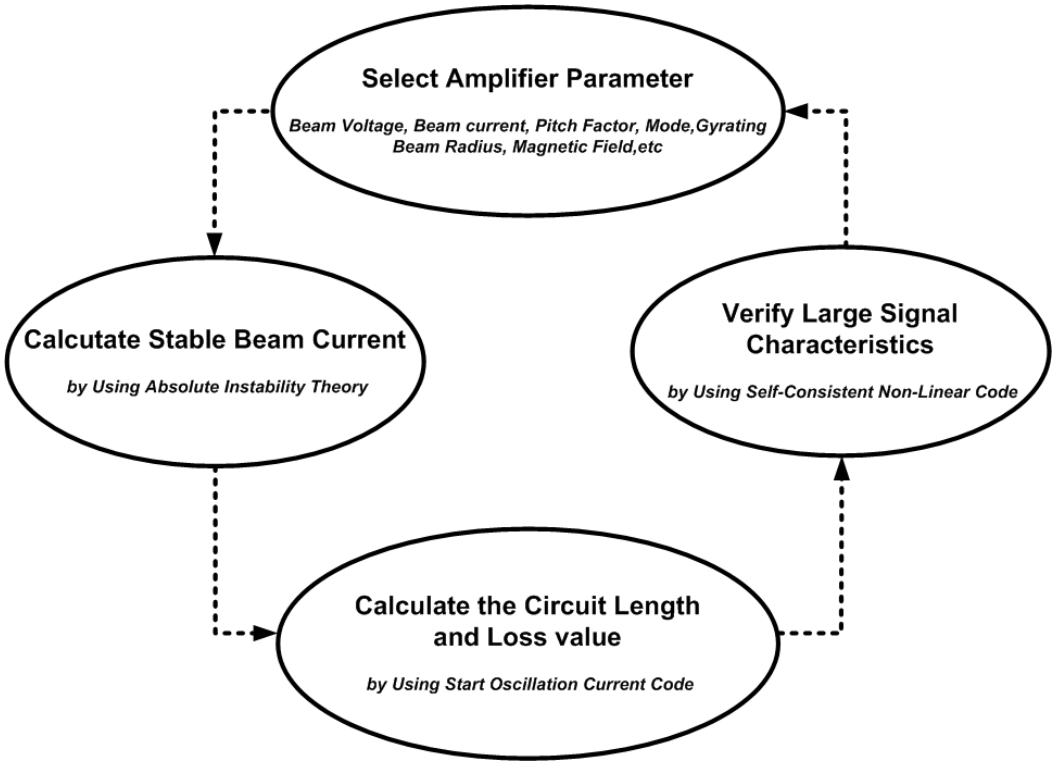

Figure 5.11. Flow chart of large signal analysis of gyro-TWT.

A mode selective RF circuit using wedge shaped lossy ceramic rods (shown in Fig. 5.1) is selected that supports an azimuthally symmetric operational TE_{02} mode. Further, it

provides the resistive loss to other TE_{0n} modes and also to azimuthally asymmetric TE_{mn} modes to suppress the oscillations. In the present study, six numbers of lossy dielectric fins are arranged in azimuth with the symmetry of 60^o to provide sufficient loss to suppress the parasitic modes. These lossy dielectric fins having sufficient thickness, increases the conversion efficiency of harmonic gyro-TWT operating in azimuthally symmetric mode greatly, as compared to the azimuthally asymmetric modes of operation. The physics of amplification and self-start parasitic oscillations are studied through the beam-wave interaction mechanism of the gyro-TWT. This is carried out using a selfconsistent nonlinear theory [Sirigiri (1999), Wang (1995)]. The design parameters of the dielectric loaded W-band second harmonic gyro-TWT are listed in the Table-5.1. The beam voltage, length of the waveguide, and the pitch of the electron beam are chosen based on the design specifications including RF output power, efficiency, gain, and estimation of start current of parasitic modes or the device stability.

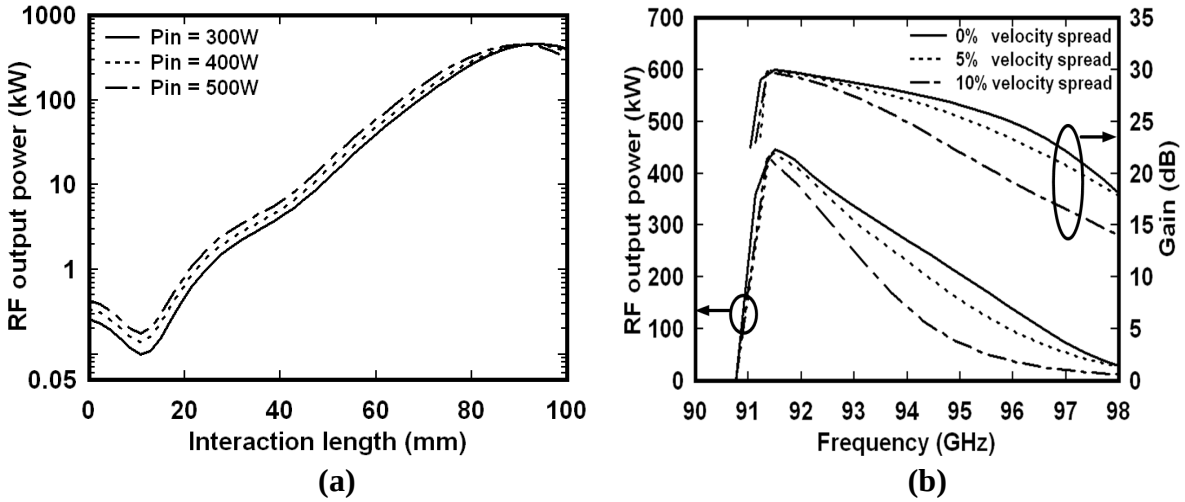

(a) **(b)**

Figure 5.12. (a) Spatial power growth in gyro-TWT amplifier for different RF driver power, and **(b)** RF output power and the saturated gain for different velocity spread.

The start current of the desired TE_{02}^2 mode is determined using the propagation loss as shown in the Fig. 5.6, which is the key requirement for the design of the gyro-TWT. The

RF circuit consists of two sections. The front part is loaded with a lossy ceramic to provide the sufficient loss and suppress the spurious parasitic modes including TE_{02}^{3}, TE_{03}^{4} and TE_{01}^{2}. In this lossy section, the gyrating electron beam is phase modulated and allowed to interact with the RF signal in the lossless air filled output section. The length of lossless unloaded section is always kept shorter than the critical length to avoid excitation of the parasitic modes, as discussed in section 5.3.

The large signal behavior of the gyro-TWT is studied using a self-consistent set of the nonlinear equations. They describe basically the change in the energy of electrons, phase of electrons and the amplitude of the RF field along the axial direction of the RF circuit. The beam-wave interaction behavior is depicted as a function of the normalized parameters including the length, detuning parameter, beam current, etc. In the present work, a self-consistent code is developed to study the nonlinear transient behavior of a W-band 2nd harmonic gyro-TWT using the wedge shaped lossy ceramic rods operated in the azimuthally symmetric TE_{02} mode. The profile of the RF amplification along the axial direction of the RF interaction circuit is shown in Fig. 5.12 (a) for a 100kV, 25A gyrating electron beams. In the gyrotron devices, velocity spread of the electron beam plays a vital role, therefore to evaluate the performance of the present harmonic gyro-TWT the beam is mathematically modeled using a Gaussian distribution function with a suitable weight. Due to the inhomogeneous Doppler broadening of the cyclotron resonance band in the axial velocity of the electron beam, the efficiency of the device decreases as shown in Fig. 5.15. As the axial velocity spread of the electrons increases, the difference in transit time of electrons increases, hence electrons interact with the RF signal field at different phases, which in turn reduces the power extraction efficiency.

In the present design studies, the RF saturated output power of ~ 450kW with a large signal gain of ~30dB is achieved for the RF input power of 450W. The power conversion efficiency of ~ 18% at 91.4GHz for 5% of axial velocity spread is obtained. The nonlinear performance of the amplifier for the different velocity spreads (0%, 5%, and 10%) is shown in Fig. 5.12 (b) and observed that the bandwidth decreases as the axial velocity spread increases.

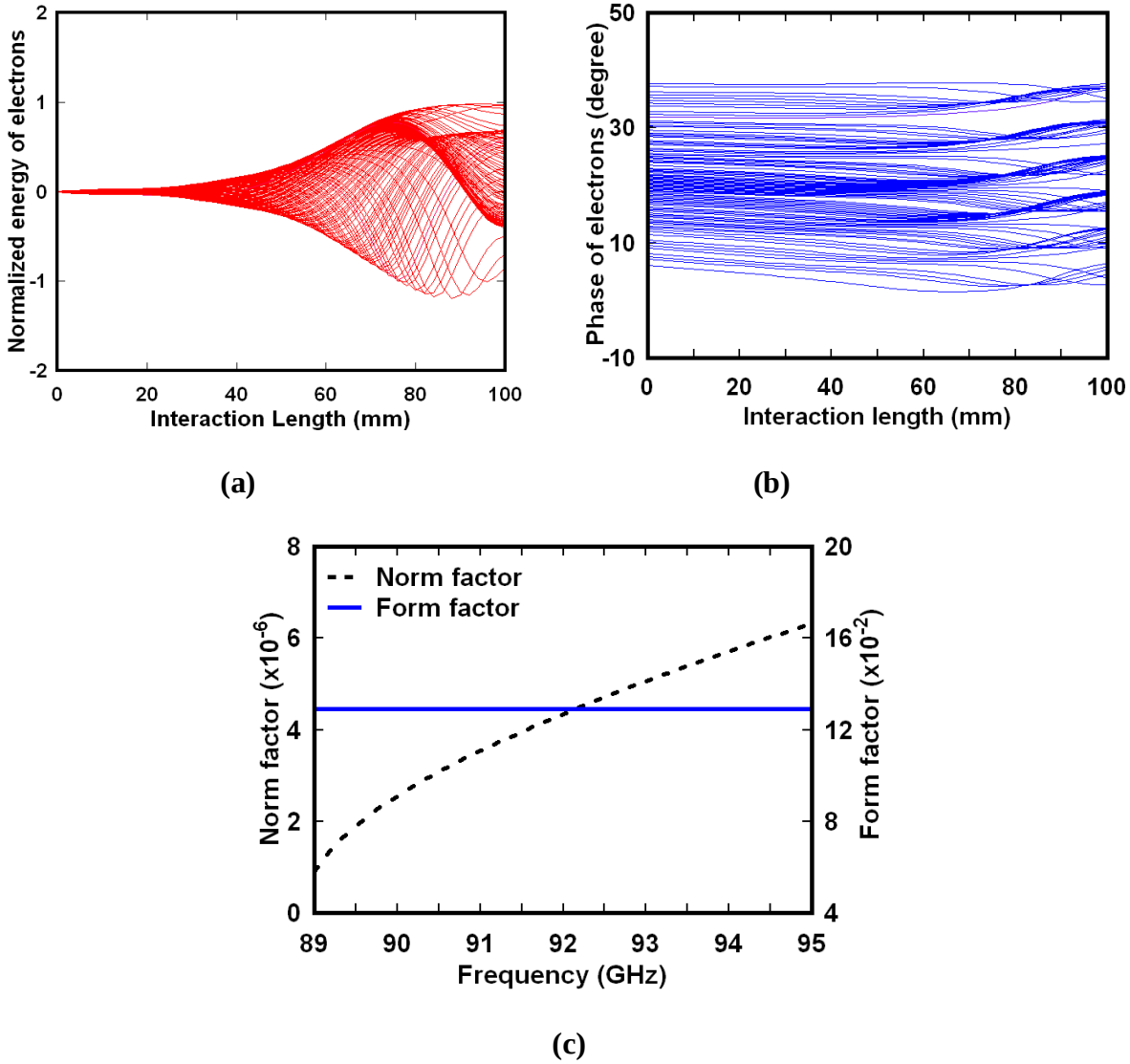

Figure 5.13. (a,b) Energy and phase variation of electrons along length of the interaction circuit for 5% velocity spread, and **(c)** variation of Norm and Form factor with frequency.

Figure 5.13(a) shows the variation of energy of electrons and describe the modulation of momentum of particles along the propagation direction in the interaction circuit. Due to phase bunching of electrons in each velocity class, the energy exchange taking place. Due to the interaction between the streaming electrons and the RF signal at the same time energy distribution of electrons changes. At the output, the net energy of electron is negative which depict that electrons transferred their energies to the wave. The bunching of all the particles exists in the nearly middle of the interaction circuit. Once electrons transferred their energy to wave, the de-bunching takes place.

Figure 5.13(b) illustrates the phase variation of electrons along the propagation direction of the interaction circuit for 5% velocity spread. Due to cyclotron resonance mismatch electron slippage with respect to the electromagnetic field. This makes a difference in the axial velocity of the beam, which in turn affect the performance of the gyro-TWT amplifier. We have considered the velocity spread as a Gaussian distribution and in which the same velocity sets of electrons are grouped together. Each of these sets is described by the weight of the Gaussian distribution and the total number of macro electrons and every velocity set has the same initial longitudinal and transverse momentum. The initial phase of electrons within each velocity set is uniformly distributed over the interval 0 to 2π and also to avoid the overlapping between different velocity sets of electrons, we have divided the phase space for each set from $2n\pi$ to $2(n+1)\pi$.

Figure 5.13 (c) shows the variation of norm factor and form factor with frequency. The form factor (L_s) refers the coupling between the cyclotron wave and the resonant waveguide mode. Form factor depends on the transverse dimension of the waveguide and operating mode but not frequency dependent, as a result for all operating frequencies, the

value of form factor will remain same as shown in Fig. 5.13(b). The norm factor (N_s) which describes the RF power propagating through the interaction circuit per unit area, is dependent on both operating mode and frequency. This increases as the operating frequency increases, as can be seen from Fig. 5.13(c). Figure 5.14 shows the performance of amplifier for the different values of the RF driver signal strength.

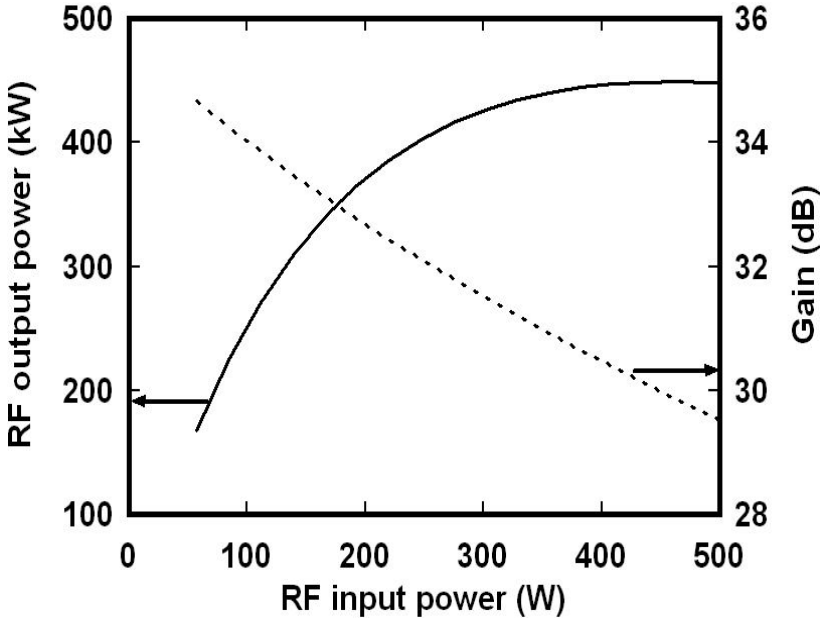

Figure 5.14. RF output power and the gain of second harmonic gyro-TWT amplifier.

5.5. PIC Simulation of a Second Harmonic W-Band Gyro-TWT Amplifier

In the present work, the interaction circuit of the W-band gyro-TWT is being loaded with six wedges of ceramic dielectric material azimuthal symmetry which suppress the spurious oscillations. This loaded interaction sectional and 3D cut view circuit has been modelled as shown in Fig. 5.15(a) to study the beam-wave interaction mechanism. The interaction region consists of two parts namely long lossy periodically azimuthally loaded and the conducting unloaded sections. The dielectric material for the loaded section of the

model has been chosen as Beryllium oxide-Silicon carbide (BeO-SiC) with a relative permeability of ε_r = *7.11-j1.1* and a relative permeability μ_r = *1* and which is a lossy material due to its good thermal conductivity and which is also importance for high average power operation. The loaded section consists of six ceramic wedges of 72mm length, and the radial thickness of the dielectric fin is 1.27mm. The unloaded section has 24mm length. Total length of the interaction circuit is 100mm. Fig. 5.15 (b) shows longitudinal electric field distribution of the desired mode along the axial direction.

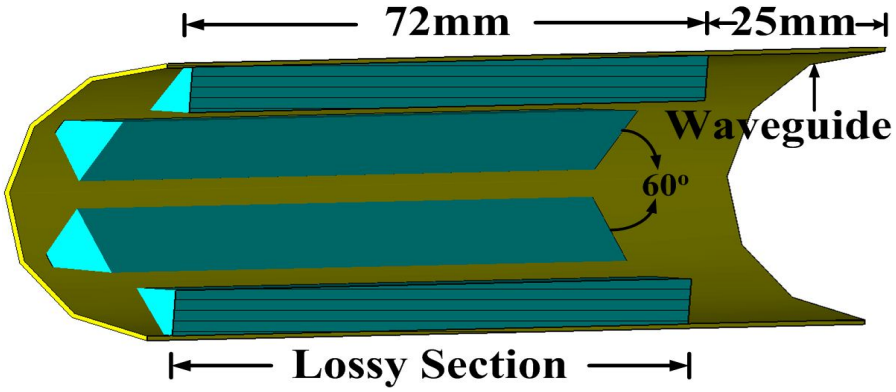

(a)

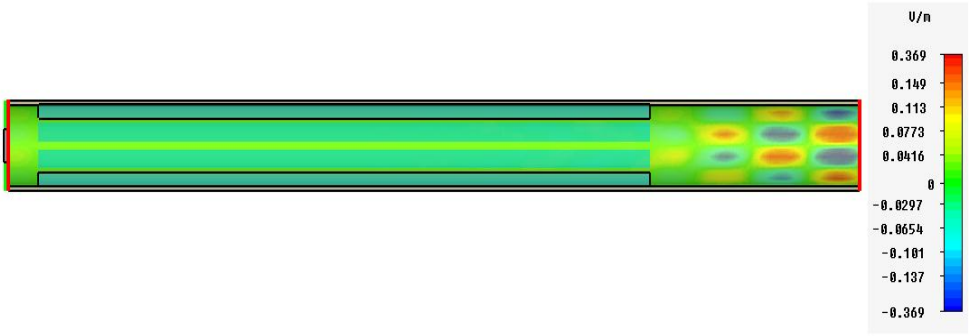

(b)

Figure 5.15. (a) Cut view of 3D simulation model of gyro-TWT amplifier, and **(b)** Side view of the contour of electric field intensity along the propagation direction of waveguide.

5.6. Result and Discussion

5.6.1. *Simulation Results and Discussion*

The beam present simulation is carried out by introducing a hallow annular gyrating electron beam having a guiding centre radius of 1.55mm into the RF interaction circuit from a DC emission model. The emitting surface is inclined at an angle of ~50° to the direction of the guiding magnetic field to provide the velocity ratio of 1.2. An absorbing boundary condition is used at the output port of the RF interaction circuit. To observe the behaviour of the parasites (including TE_{01}^{2}, TE_{02}^{3} and TE_{03}^{4} modes) which are closely competing with the desired TE_{02}^{2} operating mode, 60 modes have been set at the output port during the simulation. The presence of RF fields disturb the homogeneity of streaming electron beamlets in the RF circuit, hence the electron bunching occurs. When the bunched electrons move into the retarding phase of the RF field, the kinetic energy of electrons transfered to the RF field. The numbers of electrons gaining energy are equal to the number of electrons loosing energy at resonance, hence no net transfer of energy.

Initially all electrons have same energy of 100keV and due to the interaction with RF wave, most of the electrons have lower energy at the end of 100ns simulation period. It indicates that the energy of electrons is transferred to RF wave. In the present simulation the total number of macro electrons reached around 28,000. The temporal growth of the amplitude of the RF voltage and the corresponding power in TE_{02} mode at the output port are shown in Figs. 5.16(a) and 5.16(b), respectively, for the driver power of 450W.

The amplifier saturates around 10ns of simulation time as shown in Fig.5.16(a). Figure 5.16(b) shows the peak power of ~ 435kW, which the direct square of the voltage amplitude developed in the desired TE_{02} mode. The yellow curve in Fig.5.16(b) shows the

average power in TE_{02} mode of operation of second harmonic gyro-TWT. Further, the parasites are suppressed as shown in Fig.5.16(a) by taking the advantages of the present wedge shaped ceramic rods, therefore the stability of the amplifier is ensured.

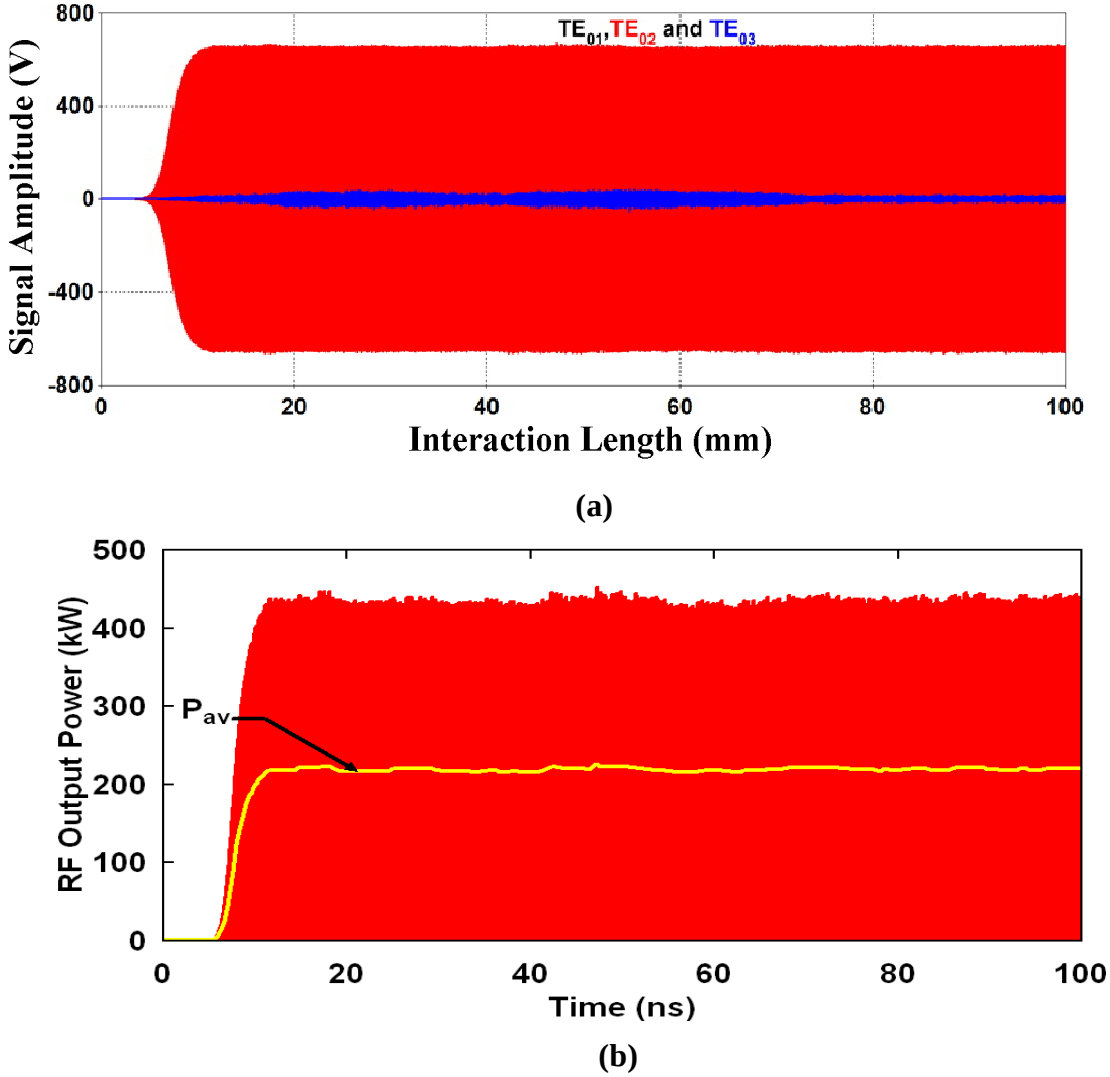

Figure 5.16. (a) Temporal response of desired and competing modes at the output port, and (**b)** Temporal power growth in TE_{02}-mode of gyro-TWT amplifier.

Figure 5.17(a) shows the probed electric field at both input and output ports which is maximum at the desired frequency of operation. Further, the frequency spectrum of the output signal is obtained by taking the Fourier transform of it as shown in Fig. 5.17(b). This

frequency spectrum is unique at 91.4GHz for the TE_{02} mode of operation and no harmonics are observed around it. This ensures that the parasites are suppressed while using the ceramic rods and hence the single mode operation of the amplifier is achieved.

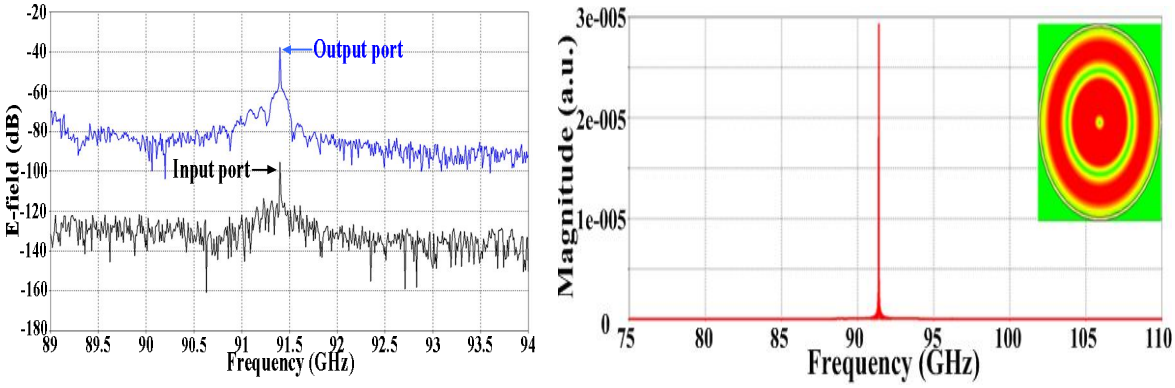

(a) **(b)**

Figure 5.17. (a) Electric field developed at both input and output ports, and **(b)** Fourier transform of the electric field depicts the operating point of gyro-TWT at 91.4GHz.

5.6.2. *Parametric Analysis and Validation*

In order to evaluate the performance of the present second harmonic gyro-TWT, its circuit and electrical parameters have been varied. Initially, the RF output power of the amplifier is observed by varying the circuit parameters including the radial thickness (r_d), length (l), and width (w_1 and w_2) of the ceramic rods. Fig.5.18 (a) shows the frequency response of the amplifier for different widths while fixing the radial thickness and length as constant.Similarly, Fig.5.18 (b) shows the variation of the RF power for different length of the ceramic wedge. These variations signify the optimized circuit parameters as w_1 = 0.4mm, w_2 = 2mm, r_d = 1.27mm, and l = 72mm, for the desired RF output power and obtain the stability against the parasites. Further, the electrical parameters including the velocity ratio, magnetic field, beam current, and input power. Figure 5.19(a) and 5.19(b) shows the variation of the peak power for different values beam pitch and the externally applied

magnetic field, respectively. The saturated gain of the amplifier is calculated as ~30dB for the pitch of 1.2 and the B-field of 1.78T.

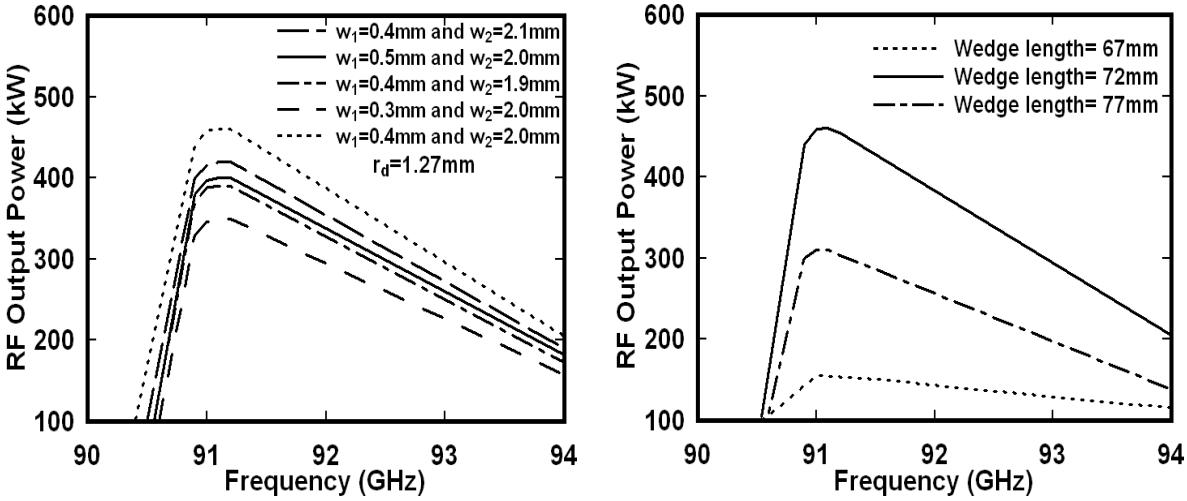

Figure 5.18. (a) Variation of RF output power with respect to frequency for different widths of the ceramic wedges while the radial thickness is fixed, and **(b)** variation of RF output power with respect to frequency different lengths of the ceramic rods.

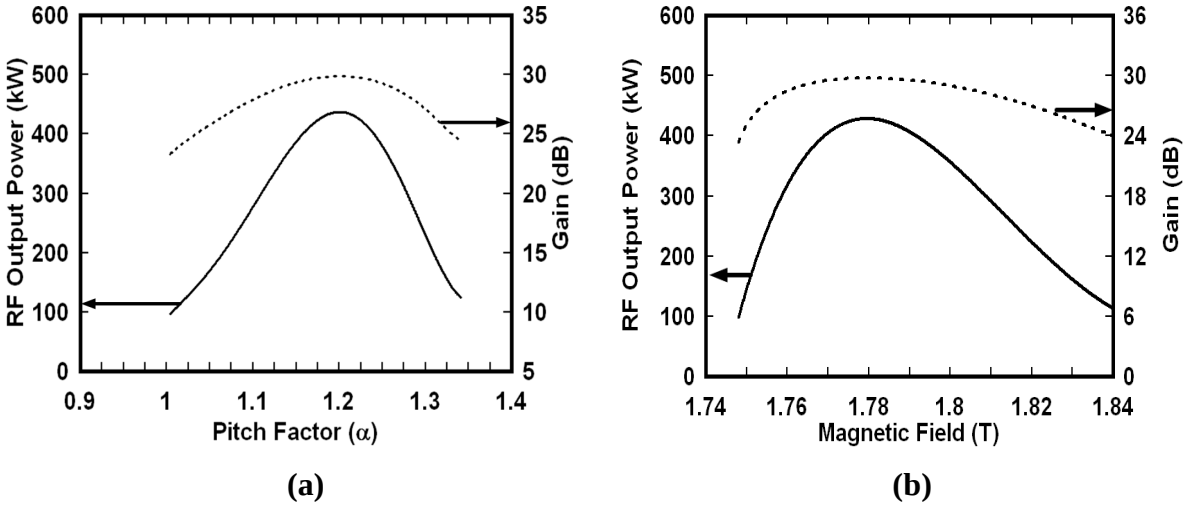

Figure 5.19. (a) Variation of RF output power and the saturated gain for different beam pitch, and **(b)** Variation of RF output power and the saturated gain for different magnetic field.

Similarly, the response of the amplifier is observed for different beam current and the RF drive power as shown in Figs. 5.20(a) and 5.20(b), respectively. For the operating

current of 25A, the power conversion is obtained as ~17% with 5% axial beam spread. Furthermore, the results obtained through the present simulation are also validated with the self-consistent nonlinear analysis. The results of are found to be within 3% agreement as shown in Fig. 5.20(c). The instantaneous bandwidth of the present second harmonic gyro-TWT is obtained as 3% about the 91.4GHz centre frequency.

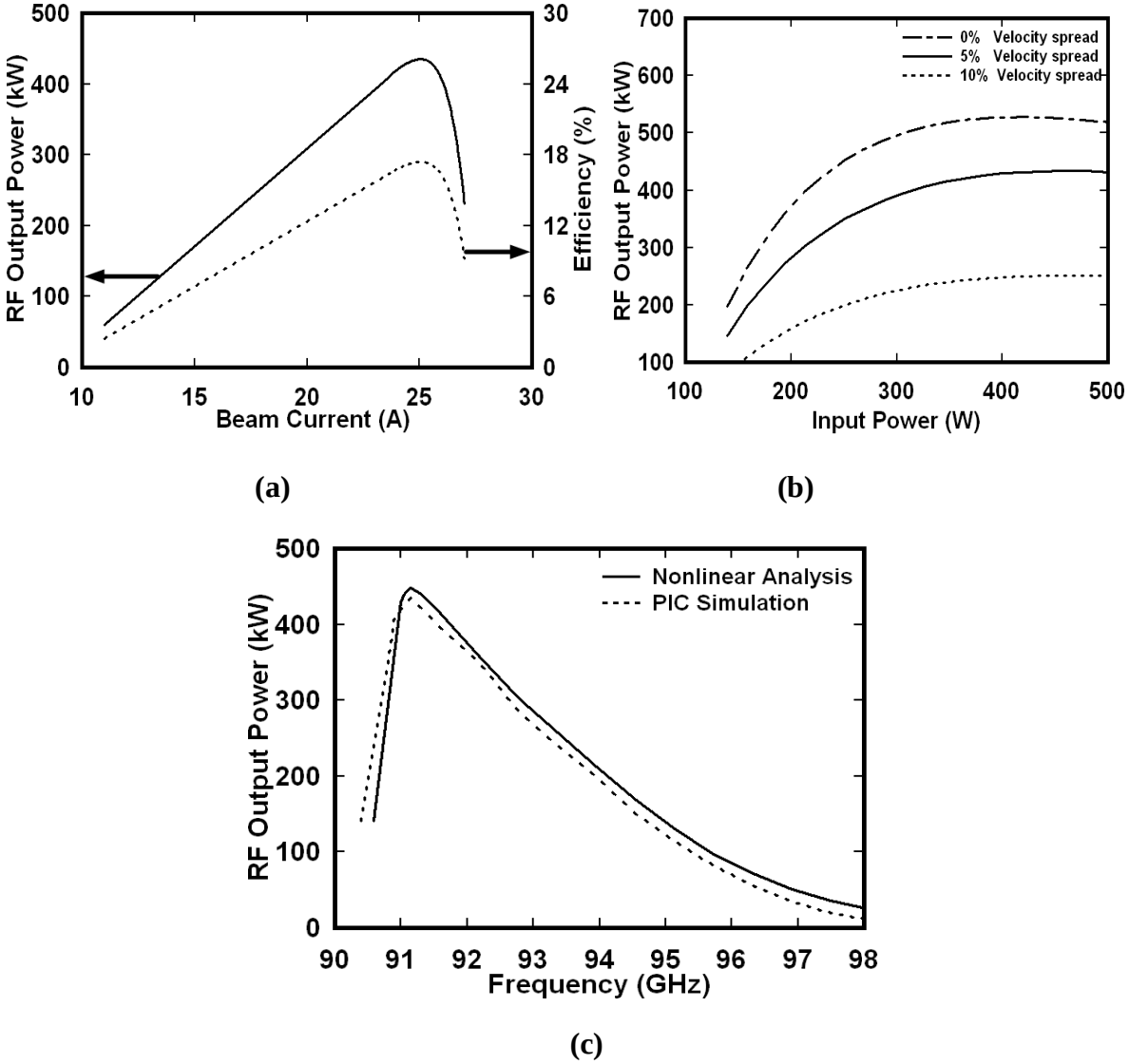

Figure 5.20. (a) Variation of peak RF power and efficiency for different beam current, **(b)** Variation of saturated RF power for various driver RF power, and **(c)** Comparison of 3D PIC and analytical responses of W-band second harmonic gyro-TWT amplifier.

5.7. Conclusion

A second harmonic gyro-TWT using the wedge shaped lossy ceramic rods loaded RF interaction circuit operating in an azimuthally symmetric TE_{02} mode has been investigated in the present Chapter. Such lossy dielectric loading leads to the mode selective behavior and proper choice of wedge dimensions has been found to control the stability condition of the device. A self-consistent nonlinear analysis has been used to investigate the beam-wave interaction behavior of the amplifier. The stability of the amplifier has also been investigated by placing six wedge shaped lossy ceramics symmetrically at 60^o spacing along the azimuth of the RF circuit. By controlling the lossy ceramic rods parameters, the condition for maintaining the stability against the absolute instability and self-start oscillations has been studied. The nonlinear analysis predicted ~ 450 kW at 91.4 GHz for the operating beam characteristics of 100kV, 25A with 5% velocity spread. A saturated gain of ~30dB and an efficiency of ~18% have been obtained for the azimuthally symmetric mode with instantaneous 3-dB bandwidth of ~3%.

Further, the results obtained through nonlinear analysis are validated through the 3D PIC simulation results obtained through CST Particle Studio. The simulation predicted a saturated RF output power of ~435kW in TE_{02} mode at 91.4GHz with an electronic efficiency ~17%, for 100kV, 25A annular electron beam having the pitch of 1.2 and the axial beam spread of 5%. The saturated gain was obtained as ~30dB with an instantaneous bandwidth of ~3%.

In the next chapter, the analysis of the gyro-TWT has been extended further to simultaneously predict present of all the modes present in the RF output of the device. For

this purpose, a time dependent multimode nonlinear analysis of gyro-TWT amplifier will be developed and applied to study the multimode behaviour of the gyro-TWT.